

# On Device Modeling for Circuit Simulation With Application to Carbon-Nanotube and Graphene Nano-Ribbon Field-Effect Transistors

Ibrahim N. Hajj, *Fellow*

**Abstract**—This paper presents a method for deriving circuit model stamp equations from the characteristic equations of multiterminal devices. The method is applied to the derivation of stamp equations of carbon nanotube and graphene nano-ribbon field-effect transistors (FETs) for use in general-purpose circuit simulators. We first review existing methods of modeling FETs for circuit simulation and point out some of the weaknesses in these models. We then explain how to derive model equation stamps directly from the device physical characteristic equations without the need of eliminating internal device variables and without having to construct equivalent circuits consisting of interconnections of two-terminal resistors, controlled sources, and two-terminal capacitors.

**Index Terms**—Carbon-nanotube FETs, circuit equation stamps, circuit models, circuit simulation, extended nodal analysis, graphene nano-ribbon FETs, MOSFETs, surface potential.

## I. INTRODUCTION

Modeling of electronic devices for circuit simulation has been an active area of research since the sixties and early seventies, especially when computer programs, such as SPICE and its derivatives [1], became widely available. In this paper, we take a critical look at circuit modeling of field-effect transistor (FET) devices, in general, and at recently proposed models of carbon nanotube and graphene nano-ribbon FETs, in particular. The focus is not on deriving circuit models of the transistors from the physics of the device, but rather on how to properly incorporate the model equations into the overall circuit equations in a general-purpose circuit simulator, without the need of eliminating internal variables from the characteristic equations and having to construct equivalent circuit models consisting of interconnections of two-terminal resistors, capacitors, and controlled sources. To understand the basis of circuit modeling of carbon nanotube and graphene nano-ribbon FETs, one has to review circuit modeling of MOSFETs. The FET is a three- or four-terminal device. The characteristics are normally derived as currents and charges in terms of terminal voltages as well as internal variables, such as the channel surface-potential, often denoted by  $\psi_s$  [5], [6]. The current in the FET channel consists of two components, a transport current (dc current) and a charging current (ac current). Both are functions of terminal voltages and internal variables. The charging current is often labeled as capacitive characteristics. The capacitive characteristics of FETs consist of overlap capacitances, junction capacitances, and intrinsic or “quantum” capacitance. Overlap and junction capacitances depend on device geometry and process parameters that are normally easily

modeled. The focus in this paper, is on circuit equation modeling of the intrinsic capacitances.

We consider four-terminal devices, where the terminals are labeled  $G$  for gate,  $S$  for source,  $D$  for drain, and  $B$  bulk, body, backgate or substrate, in the case of four-terminal devices. We denote the charge in the channel, referred to as quantum charge, as  $Q_{CNT}$  or  $Q_{CH}$  interchangeably; and the surface potential as  $\Psi_S$ ,  $\Phi_B$ ,  $V_{CH}$ , and  $v_{CH}$  based on the notation used by different authors. The surface-potential has been found to be a key parameter in modeling the FET characteristics. It is a nonlinear function of the terminal voltages and is an important parameter in determining the dc current and the charge variations in the channel [5], [6]. The general approach followed in all existing methods in circuit modeling of FETs, including MOSFETs, is to first eliminate the surface-potential variable and express the charges in terms of two-terminal (nonlinear) capacitor network connecting the terminal nodes.

Raychowdhury *et al.* [7] considered the modeling of three-terminal ballistic carbon nanotube field-effect transistors. They derive an equation for  $Q_{CNT}$  in term of  $v_{DS}$  and  $\Psi_S$ , and an equation of  $\Psi_S$  in terms of  $v_{GS}$  and  $v_{DS}$  using curve-fitting techniques.  $\Psi_S$  can then be eliminated from the dc channel current  $I_{DS}$  equation to give an expression in terms of  $v_{GS}$  and  $v_{DS}$  only. The capacitance is found by differentiating  $Q_{CNT}$  with respect to  $v_{GS}$ . The capacitance  $C_G$  is then split into two capacitances  $C_{GS}$  connecting  $G$  to  $S$ , and  $C_{GD}$  connecting  $G$  to  $D$ , in the same way that  $Q_{CNT}$  is split into  $Q_S$  and  $Q_D$ , as is done in [3]. It is obvious that the circuit model is not complete. The dependence of  $Q_{CNT}$  on  $v_{DS}$  and  $\Psi_S$  is ignored.

Deng and Wong [8], [9] derived a circuit model of the intrinsic channel region of a carbon-nanotube field-effect transistor. The current in the channel is derived in terms of the terminal voltages and  $\Delta\Phi_B$ , the channel surface-potential change in response to changes in gate, source, and drain bias.  $\Delta\Phi_B$  is determined by using charge conservation equation

$$Q_{cap} = Q_{CNT} \quad (1)$$

where  $Q_{cap}$  is the total charge in the gate to channel capacitance, substrate to channel capacitance, and between the channel and the external drain and source terminals. Both  $Q_{cap}$  and  $Q_{CNT}$  are functions of the terminal voltages and  $\Delta\Phi_B$ . Equation (1) is solved iteratively by using a “construct” or side circuit to find  $\Delta\Phi_B$  for given values of the terminal node voltages. The construct circuit is connected to the  $D$  terminal. The solution of  $\Delta\Phi_B$  of the construct circuit is used to eliminate  $\Delta\Phi_B$  from the  $I_{DS}$  equation. The capacitive model of the transistor is obtained by first partitioning  $Q_{CNT}$  into  $Q_D + Q_S$ . The capacitive model is obtained by differentiating the charge equations with respect to the terminal voltages,  $C_{ij}(v) = |\partial Q_i / \partial v_j|$ , where  $C_{ij}$  is a two-terminal capacitor connecting node  $i$  to node  $j$ , as proposed in [3] and [5]. No mention is given about  $C_{ii} = |\partial Q_i / \partial v_i|$ . There are some shortcomings in this circuit model: 1) by connecting the construct circuit to the drain terminal  $D$  will add an unwanted extra term in the KCL equation at  $D$  and

Manuscript received June 27, 2014; revised December 6, 2014; accepted December 18, 2014. Date of publication January 12, 2015; date of current version February 17, 2015. This paper was recommended by Associate Editor A. Srivastava.

The author is with the Coordinated Science Laboratory, Department of Electrical and Computer Engineering, University of Illinois at Urbana-Champaign, Urbana, IL 61801-2307 USA, and also with the American University of Beirut, Beirut 1107-2020, Lebanon (e-mail: ihajj@illinois.edu). Digital Object Identifier 10.1109/TCAD.2014.2387864

2) representing  $\partial Q_i/\partial v_j$  by a capacitance  $C_{ij}(v)$  connecting nodes  $i$  and  $j$  produces errors in the circuit equations, as we show in the next section.

Chen *et al.* [10], [11] derived a SPICE model for graphene nano-ribbon FET. They follow a method similar to the one proposed in [8]. The surface-potential  $V_{CH}$  in the channel is represented by a node connected to ground by a voltage-controlled voltage source equal to  $V_{CH}$ .  $V_{CH}$  is found by solving a side circuit that implements the equation  $Q_{CAP} = Q_{CH}$ , as is done in [8]. The complete SPICE model consists of  $I_{DS}$ , the voltage-controlled voltage source  $V_{CH}$  connecting the channel node to ground, the side circuit connected to  $G$ , and four capacitances,  $C_G$ ,  $C_B$ ,  $C_{CH,S} = \partial Q_{CH}/\partial v_S$ , and  $C_{CH,D} = \partial Q_{CH}/\partial v_D$ , connected from the terminals  $G$ ,  $B$ ,  $S$ , and  $D$  to the channel node  $V_{CH}$ , respectively. The shortcomings of the model are as follows: 1) the side circuit is connected to gate terminal  $G$ , which adds to the KCL equation at the gate terminal an extra current component that does not exist in the original circuit; 2) the voltage-controlled voltage source connecting  $V_{CH}$  to ground introduces a current variable from the channel to ground that does not exist in the original model; and 3) the dependence of the charge  $Q_{CH}$  at  $S$  on  $v_D$  and at  $D$  on  $v_S$  are ignored.

Frégonèse *et al.* [12] and Najari *et al.* [13] proposed a compact model of a three-terminal schottky barrier carbon nanotube transistor. The surface potential voltage, denoted by  $v_{CH}$ , is represented by a separate node, which is connected to the terminal nodes by linear capacitors and current sources  $dQ_D/dt$  and  $dQ_S/dt$ . The KCL equation at node  $v_{CH}$  is used to determine  $v_{CH}$ . Unfortunately, the circuit model configuration produces a floating  $v_{CH}$  node during dc analysis, which results in a singular circuit matrix and an undefined value for  $v_{CH}$ . In addition, no SPICE compatible circuit model is given.

Thiele *et al.* [14] modeled the quantum capacitance at a point  $x$  in the graphene FET channel as  $C_q = -dQ_{sh}/dV_{CH}$ , where  $V_{CH}$  is the channel surface-potential at  $x$  and  $Q_{sh}$  is the overall mobile sheet charge density and is a function of  $V_{CH}$ .  $Q_{sh}$  is then approximated as  $Q_{sh} = -1/2C_q V_{CH} = 1/2(dQ_{sh}/dV_{CH})V_{CH}$ . The linearized charge conservation equation at a node  $x$  in the channel is expressed in terms of  $V(x)$ ,  $V_{CH}$ ,  $v_{GS}$ , and  $v_{BS}$ , where  $V(x)$  is the voltage drop in the graphene channel. By integrating from the source  $S$  to the drain  $D$  over the channel, the current  $I_{DS}$  and the net channel charge  $Q_{CH}$  are obtained in terms of  $v_{GS}$ ,  $v_{BS}$ , and  $v_{DS}$ . The small-signal model given includes two capacitances only,  $C_{gd} = -(\partial Q_{CH}/\partial v_{DS})$  connecting  $G$  to  $D$  and  $C_{gs} = -(\partial Q_{CH}/\partial v_{GS})$  connecting  $G$  to  $S$ . The back gate  $B$  and the capacitances  $C_G$  and  $C_B$  are ignored. It is obvious that  $C_q$  is the second term of the Taylor series expansion of  $Q_{sh}$  with respect to  $V_{CH}$ , and the value  $V_{CH}$  obtained by a single solution of a linearized charge equation may not be accurate. In addition, the capacitive model in terms of  $C_{gs}$  and  $C_{gd}$  only is not complete.

Jiménez and Moldovan [15] and Jiménez [16] used a similar model to the one proposed in [14], but they consider  $C_q$  as a linear function of  $V_{CH}$ ,  $C_q = k|V_{CH}|$ , which may not be the case. This gives an explicit solution of  $V_{CH}$  in terms of  $v_{GS}$ ,  $v_{BS}$ , and  $V(x)$ , and allows the elimination of  $V_{CH}$  and  $V(x)$  from the current and charge equations. A linearized capacitive model follows the model proposed in [5], and the components are derived as partial derivatives of  $Q_G$  and  $Q_D$ . No SPICE level circuit model is included. The main shortcoming of the model is similar to [14] in that the derivative of the charge in the channel,  $C_q$ , is not a linear function of  $V_{CH}$ .

It is clear from the above review that there is a large variation in the derived circuit models and in many cases, the final capacitive circuit model is different from the initial capacitive model used in deriving the charge equations. In some cases, the derived models may not be general enough to be suitable for dc, transient, and steady-state

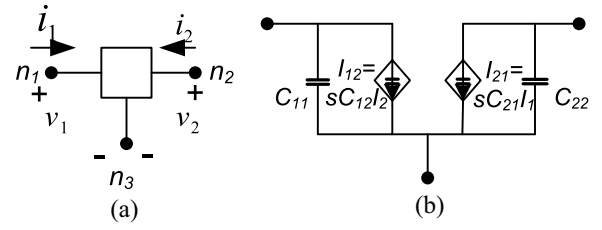


Fig. 1. (a) Three-terminal element. (b) Circuit model of a three-terminal capacitor.

analyses. In addition, the circuit equations using the derived circuit models may not satisfy the original model equations.

In the next section, we review a general method of deriving circuit equation “stamps” of general multiterminal capacitors from the element characteristic equations for use in a general purpose circuit simulator, and give some observations in Section III. In Section IV, we explain how to derive circuit equation stamps of carbon nanotube and graphene nano-ribbon FETs from the device basic equations without the need to eliminate the internal surface potential variable  $\Psi_S$  and without having to derive an equivalent circuit model consisting of two-terminal circuit elements, such as resistors, capacitors, and controlled sources. The conclusion is given in Section V.

## II. MULTITERMINAL CAPACITORS

In this section, we review characteristic equations and circuit models of multiterminal capacitors, which is relevant to the circuit modeling of the intrinsic capacitance of transistors, before we address the circuit modeling of carbon-nanotube and graphene nano-ribbon FETs in Section III.

For simplicity, we consider a three-terminal capacitor, with nodes  $n_1$ ,  $n_2$ , and  $n_3$ , as shown in Fig. 1(a). Extension to multiterminal capacitors with more than three terminals is straight-forward. Let the capacitor be characterized by a relationship between charge  $q$  and voltage  $v$

$$q_1 = f_1(v_1, v_2), \quad i_1 = \frac{dq_1}{dt} \quad (2)$$

$$q_2 = f_2(v_1, v_2), \quad i_2 = \frac{dq_2}{dt} \quad (3)$$

where node  $n_3$  is chosen as a reference node. When performing transient analysis, if the Backward Euler (B.E.) formula is applied to (2) and (3) at time  $t_n$ , one gets<sup>1</sup>

$$i_{1(n)} = \frac{1}{h} [f_1(v_{1(n)}, v_{2(n)}) - q_{1(n-1)}] \quad (4)$$

$$i_{2(n)} = \frac{1}{h} [f_2(v_{1(n)}, v_{2(n)}) - q_{2(n-1)}] \quad (5)$$

where for  $j = 1, 2$ ,  $i_{j(n)}$  and  $f_j(v_{1(n)}, v_{2(n)})$  are the values of  $i_j$  and  $f_j(v_1, v_2)$  at time  $t_n$ , respectively,  $q_{j(n-1)}$  is the value of  $q_j$  at time  $t_{n-1}$ , and  $h = t_n - t_{n-1}$  is the timestep. If Newton iterative method is applied to solve the circuit equations at time  $t_n$ , the nonlinear equations are linearized at an iteration point  $x_n^{(k)}$ , where  $x$  represents the circuit variables, using the first two terms of Taylor series expansion, provided the equations are differentiable at  $x_n^{(k)}$ . The linearization of (4) and (5) at  $v_{1(n)}^{(k)}$  and  $v_{2(n)}^{(k)}$  at iteration  $(k)$  yields equations of the form

$$i_{1(n)} = \frac{1}{h} \left( a_1^{(k)} v_{1(n)} + b_1^{(k)} v_{2(n)} + c_1^{(k)} - q_{1(n-1)} \right) \quad (6)$$

$$i_{2(n)} = \frac{1}{h} \left( a_2^{(k)} v_{1(n)} + b_2^{(k)} v_{2(n)} + c_2^{(k)} - q_{2(n-1)} \right). \quad (7)$$

<sup>1</sup>Other linear multistep formulas can be applied as well [18].

If the circuit equations are constructed using the nodal equation formulation method, the corresponding stamp of (6) and (7) would be

$$\frac{1}{h} \begin{bmatrix} +a_1^{(k)} & +b_1^{(k)} & -d_1^{(k)} \\ +a_2^{(k)} & +b_2^{(k)} & -d_2^{(k)} \\ -a_3^{(k)} & -b_3^{(k)} & +d_3^{(k)} \end{bmatrix} \begin{bmatrix} v_{n1} \\ v_{n2} \\ v_{n3} \end{bmatrix} \quad (8)$$

where  $d_1^{(k)} = (a_1^{(k)} + b_1^{(k)})$ ,  $d_2^{(k)} = (a_2^{(k)} + b_2^{(k)})$ ,  $a_3^{(k)} = (a_1^{(k)} + a_2^{(k)})$ ,  $b_3^{(k)} = (b_1^{(k)} + b_2^{(k)})$ , and  $d_3^{(k)} = (d_1^{(k)} + d_2^{(k)})$ . The contribution to the right-hand side vector is given by

$$\frac{1}{h} \begin{bmatrix} -c_1^{(k)} + q_{1(n-1)} \\ -c_2^{(k)} + q_{2(n-1)} \\ c_1^{(k)} - q_{1(n-1)} + c_2^{(k)} - q_{2(n-1)} \end{bmatrix}. \quad (9)$$

In small-signal steady-state analysis, (2) and (3) become

$$I_1 = sC_{11}V_1 + sC_{12}V_2 \quad (10)$$

$$I_2 = sC_{21}V_1 + sC_{22}V_2 \quad (11)$$

where  $s = j\omega$ ,  $C_{11} = \partial f_1/\partial v_1$ ,  $C_{12} = \partial f_1/\partial v_2$ ,  $C_{21} = \partial f_2/\partial v_1$ , and  $C_{22} = \partial f_2/\partial v_2$ , evaluated at an operating point, and the nodal equation stamp becomes

$$s \begin{bmatrix} +C_{11} & +C_{12} & -C_{13} \\ +C_{21} & +C_{22} & -C_{23} \\ -C_{31} & -C_{32} & +C_{33} \end{bmatrix} \begin{bmatrix} V_{n1} \\ V_{n2} \\ V_{n3} \end{bmatrix} \quad (12)$$

where  $C_{13} = (C_{11} + C_{12})$ ,  $C_{23} = (C_{21} + C_{22})$ ,  $C_{31} = (C_{11} + C_{21})$ ,  $C_{32} = (C_{12} + C_{22})$ , and  $C_{33} = (C_{13} + C_{23}) = (C_{31} + C_{32}) = (C_1 + C_2 + C_3 + C_4)$ . A circuit diagram representing (10) and (11) will consist of the parallel connections of capacitors and ‘‘voltage-controlled capacitive current sources,’’ as shown in Fig. 1(b). Such a controlled source has been used in [5] in modeling the capacitance of FETs at high frequency. However, such equivalent circuits are not necessary to formulate the circuit equations.

### III. OBSERVATIONS

#### A. Observation 1

The concept of modeling multiterminal resistors and inductors by including controlled elements, namely, dependent sources and mutual inductance, has been widely used, but the use of dependent capacitors in modeling multiterminal capacitors has not caught on.

#### B. Observation 2

In formulating the characteristic equations (2) and (3), any node,  $n_1$ ,  $n_2$ ,  $n_3$ , or ground node, could have been chosen as the reference node. Different reference nodes result in different equivalent circuits, but it can be shown that the stamp remains the same, irrespective of the reference node chosen.

#### C. Observation 3

This observation is concerned with the time-domain circuit modeling of nonlinear capacitors and inductors, that is, elements with differential operators in their characteristic equations. We will illustrate with a two-terminal nonlinear capacitor. The observation applies to multiterminal elements as well. Given a nonlinear capacitor with characteristics

$$q = f(v), \quad i = \frac{dq}{dt} \quad (13)$$

$$i = \frac{df(v)}{dt} = C(v) \frac{dv}{dt} \quad (14)$$

where  $C(v) = df(v)/dv$  is a nonlinear function of  $v$ . Note that  $C(v)$  is the second term of a Taylor series expansion of  $f(v)$ . In many cases

in literature, the capacitance  $C(v)$  is specified rather than  $f(v)$ . In this case, the equations used for transient analysis will not be complete. For example, if the B.E. formula is used in finding the transient response, the discretized and linearized charge (13) becomes

$$i_{(n)} = \frac{1}{h} C(v_{(n)}^{(k)}) v_{(n)} + \frac{1}{h} \left[ f(v_{(n)}^{(k)}) - C(v_{(n)}^{(k)}) v_{(n)}^{(k)} - q_{(n-1)} \right] \quad (15)$$

while the discretized capacitor (14) becomes

$$i_{(n)} = \frac{1}{h} C(v_{(n)}) v_{(n)} - \frac{1}{h} C(v_{(n)}) v_{(n-1)} \quad (16)$$

which is different from (15).

#### D. Observation 4

Given a multiterminal capacitor that is characterized by an equation of the form  $q = f(v)$ . Let  $C = \partial q/\partial v$  be the linearized capacitance matrix. If  $C_{ij} = \partial q_i/\partial v_j$  is connected between nodes  $i$  and  $j$ , as is done in [3], [5], [8], and [9], then the circuit equations will not be correct. We will illustrate by using the equations of a three-terminal capacitor given in (2) and (3). If  $C_{ij} = \partial q_i/\partial v_j$  is chosen as a two-terminal capacitor connected between nodes  $i$  and  $j$ , then the small-signal sinusoidal steady-state analysis circuit stamp would be

$$s \begin{bmatrix} +C_{aa} & -C_{ab} & -C_{ac} \\ -C_{ab} & +C_{bb} & -C_{bc} \\ -C_{ac} & -C_{bc} & +C_{bb} \end{bmatrix} \begin{bmatrix} V_1 \\ V_2 \\ V_3 \end{bmatrix} \quad (17)$$

where  $C_{aa} = (C_{12} + C_{21} + C_{13} + C_{31})$ ,  $C_{ab} = (C_{12} + C_{21})$ ,  $C_{ac} = (C_{13} + C_{31})$ ,  $C_{bb} = (C_{12} + C_{21} + C_{23} + C_{32})$ ,  $C_{bc} = (C_{23} + C_{32})$ , and  $C_{cc} = (C_{13} + C_{31} + C_{23} + C_{32})$ . Note that the matrix is symmetric and  $C_{11}$ ,  $C_{22}$ , and  $C_{33}$  do not appear in the matrix; they have been shorted out. On the other hand, the correct circuit stamp is given in (12).

### IV. MODELING OF CARBON-NANOTUBE AND GRAPHENE NANO-RIBBON FETs FOR CIRCUIT SIMULATION

As mentioned in Section I, in circuit modeling of carbon-nanotube and graphene nano-ribbon FETs, the current and charge equations are derived in terms of  $v_G$ ,  $v_D$ ,  $v_S$ ,  $v_B$ , and the channel potential  $\Psi_S$ . Without loss of generality, we will ignore the series resistances in the gate, source, and drain and the flatband voltage in the gate. We will choose the source terminal  $S$  as the reference node. Any other node can be selected as a reference node. The channel potential  $\Psi_S$  is referenced to ground as in [8]–[11], although it can be referenced to  $S$  or  $B$  or any other node as well. The equations are then of the form (see [8])

$$i_{DS} = f_{DS}(v_{DS}, \Psi_S) \quad (18)$$

$$Q_G = C_G(v_{GS} - \Psi_S) \quad (19)$$

$$Q_B = C_B(v_{BS} - \Psi_S) \quad (20)$$

$$Q_D = f_D(v_{DS}, \Psi_S) \quad (21)$$

$$Q_S = f_S(v_{DS}, \Psi_S) \quad (22)$$

$$Q_G + Q_B + Q_D + Q_S = 0 \quad (23)$$

where the quantum charge in the channel is  $Q_{CH} = Q_D + Q_S = f_{CH}(v_{DS}, \Psi_S)$ . Equation (23) is normally used to determine  $\Psi_S$  [8]–[11]. Note that  $I_{DS}$ ,  $Q_D$ , and  $Q_S$  are also functions of  $v_{GS}$  and  $v_{BS}$  through  $\Psi_S$ .

In the following, we will derive equation stamps to be used in circuit equation formulation for dc, transient, and sinusoidal steady-state analyses.

### A. DC Analysis

At the dc point  $dQ/dt = 0$ , and the equations then become (18) and (23) only. The linearization of (18) and (23) at iteration  $(k)$  yields linearized equations of the form

$$i_{DS} = g_{DS}^{(k)} v_{DS} + g_{\Psi}^{(k)} \Psi_S + r_{DS}^{(k)} \quad (24)$$

$$C_G(v_{GS} - \Psi_S) + C_B(v_{BS} - \Psi_S) + c_{DS}^{(k)} v_{DS} + c_{\Psi}^{(k)} \Psi_S + r_{CH}^{(k)} = 0. \quad (25)$$

The coefficients in (24) and (25) are given in the Appendix. The corresponding stamp in an Extended Nodal Analysis (ENA) formulation [17] is

$$\begin{bmatrix} 0 & 0 & 0 & 0 & 0 \\ 0 & 0 & 0 & 0 & 0 \\ 0 & 0 & +g_{DS}^{(k)} & -g_{DS}^{(k)} & +g_{\Psi}^{(k)} \\ 0 & 0 & -g_{DS}^{(k)} & +g_{DS}^{(k)} & -g_{\Psi}^{(k)} \\ +C_G & +C_B & +c_{DS}^{(k)} & -d_S^{(k)} & +d_{\Psi}^{(k)} \end{bmatrix} \begin{bmatrix} v_G \\ v_B \\ v_D \\ v_S \\ \Psi_S \end{bmatrix} \quad (26)$$

where  $d_S^{(k)} = (c_{DS}^{(k)} + C_G + C_B)$  and  $d_{\Psi}^{(k)} = (c_{\Psi}^{(k)} - C_G - C_B)$ . The contribution to the right-hand side vector is given by

$$\begin{bmatrix} 0 & 0 & -r_{DS}^{(k)} & +r_{DS}^{(k)} & -r_{CH}^{(k)} \end{bmatrix}^T. \quad (27)$$

Note that the charge (23) is included in the computation of the dc solution. Note also that  $\Psi_S$  is retained as a circuit variable.

### B. Transient Analysis

In performing transient analysis and assuming B.E. formula is applied to (19)–(22) at time  $t_n$ , and linearizing the equations at an iteration point  $x_n^{(k)}$ , yields linearized equations of the form

$$i_{DS(n)} = g_{DS}^{(k)} v_{DS(n)} + g_{\Psi}^{(k)} \Psi_{S(n)} + r_{DS}^{(k)} \quad (28)$$

$$i_{G(n)} = \frac{1}{h} [C_G(v_{GS(n)} - \Psi_{S(n)}) - Q_{G(n-1)}] \quad (29)$$

$$i_{B(n)} = \frac{1}{h} [C_B(v_{BS(n)} - \Psi_{S(n)}) - Q_{B(n-1)}] \quad (30)$$

$$i_{D(n)} = \frac{1}{h} [(c_D^{(k)} v_{DS(n)} + e_D^{(k)} \Psi_{S(n)} + r_{D(n)}^{(k)}) - Q_{D(n-1)}] \quad (31)$$

$$i_{S(n)} = \frac{1}{h} [(c_S^{(k)} v_{DS(n)} + e_S^{(k)} \Psi_{S(n)} + r_{S(n)}^{(k)}) - Q_{S(n-1)}] \quad (32)$$

$$C_G(v_{GS(n)} - \Psi_{S(n)}) + C_B(v_{BS(n)} - \Psi_{S(n)}) + c_{DS}^{(k)} v_{DS(n)} + c_{\Psi}^{(k)} \Psi_{S(n)} + r_{CH}^{(k)} = 0 \quad (33)$$

where the coefficients of (28) and (33) are the same as in (24) and (25), except that they are evaluated at  $x_n^{(k)}$ . The coefficients of (31) and (32) are given in the Appendix. Note that from (23),  $i_{S(n)} = -(i_{G(n)} + i_{B(n)} + i_{D(n)})$ . The corresponding stamp in an ENA formulation [17] is of the form

$$\left[ \mathbf{G} + \frac{1}{h} \mathbf{C} \right] \mathbf{v}, \mathbf{b} \quad (34)$$

where  $\mathbf{v} = [v_G, v_B, v_D, v_S, \Psi_S]$ , and where

$$\mathbf{G} = \begin{bmatrix} 0 & 0 & 0 & 0 & 0 \\ 0 & 0 & 0 & 0 & 0 \\ 0 & 0 & +g_{DS}^{(k)} & -g_{DS}^{(k)} & +g_{\Psi}^{(k)} \\ 0 & 0 & -g_{DS}^{(k)} & +g_{DS}^{(k)} & -g_{\Psi}^{(k)} \\ +C_G & +C_B & +c_{DS}^{(k)} & -d_S^{(k)} & +d_{\Psi}^{(k)} \end{bmatrix} \quad (35)$$

and

$$\mathbf{C} = \begin{bmatrix} +C_G & 0 & 0 & -C_G & -C_G \\ 0 & +C_B & 0 & -C_B & -C_B \\ 0 & 0 & +c_D^{(k)} & -c_D^{(k)} & +e_D^{(k)} \\ 0 & 0 & +c_S^{(k)} & -c_S^{(k)} & +e_S^{(k)} \\ 0 & 0 & 0 & 0 & 0 \end{bmatrix}. \quad (36)$$

The contribution to the right-hand side vector is given by

$$\mathbf{b} = \begin{bmatrix} +\frac{Q_{G(n-1)}}{h} \\ +\frac{Q_{B(n-1)}}{h} \\ -r_{DS}^{(k)} + \frac{Q_{D(n-1)}}{h} - \frac{r_D^{(k)}}{h} \\ +r_{DS}^{(k)} + \frac{Q_{S(n-1)}}{h} - \frac{r_S^{(k)}}{h} \\ -r_{CH}^{(k)} \end{bmatrix}. \quad (37)$$

Stamps (35)–(37) do not include the contributions of the extrinsic capacitances of the device, which should be added.

### C. Small-Signal Sinusoidal Steady-State Analysis

When performing small-signal analysis, the device characteristic equations are linearized at an operating point to generate a stamp of the form

$$[\mathbf{G} + s\mathbf{C}]\mathbf{v} \quad (38)$$

where  $G$  and  $C$  are given in (35) and (36) evaluated at the dc solution.

## V. CONCLUSION

In this paper, we briefly reviewed existing methods of modeling FETs for circuit simulation and pointed out some of the weaknesses in these models, especially in the circuit modeling the FET channel charges in general, and the circuit modeling of carbon nanotube and graphene nano-ribbon FETs in particular. In many cases the derived equivalent circuit models do not conform with the original device equations. The proposed circuit model derived in this paper, is in the form of stamp equations that can be obtained from the original characteristic equations of the device without the need to eliminate internal variables and without having to construct an equivalent circuit model in terms of two-terminal resistors, capacitors, and controlled sources. The stamps are derived for dc, transient, and sinusoidal steady-state analyses. The stamps can be incorporated into the circuit equations of a circuit simulator in a straightforward manner. The method allows model developers to evaluate the performance of the validity of the device model directly from the physical device equations. Circuit designers can monitor internal device parameters since they are part of the circuit variable set. Although we have focused on circuit equation modeling of carbon nanotube and graphene nano-ribbon FETs, the same observations and results apply to MOSFET circuit modeling.

### APPENDIX

Coefficients of (24):  $g_{DS}^{(k)} = \partial f_{DS} / \partial v_{DS}$ ,  $g_{\Psi}^{(k)} = \partial f_{DS} / \partial \Psi_S$ , both evaluated at  $\mathbf{x}^{(k)}$ , and  $r_{DS}^{(k)} = f_{DS}(v_{DS}^{(k)}, \Psi_S^{(k)}) - (g_{DS}^{(k)} v_{DS}^{(k)} + g_{\Psi}^{(k)} \Psi_S^{(k)})$ .

Coefficients of (25):  $c_{DS}^{(k)} = \partial f_{CH} / \partial v_{DS}$ ,  $c_{\Psi}^{(k)} = \partial f_{CH} / \partial \Psi_S$ , both evaluated at  $\mathbf{x}^{(k)}$ , and  $r_{CH}^{(k)} = f_{CH}(v_{DS}^{(k)}, \Psi_S^{(k)}) - c_{CH}^{(k)} v_{DS}^{(k)} - c_{\Psi}^{(k)} \Psi_S^{(k)}$ .

Coefficients of (31) and (32):  $c_X^{(k)} = \partial f_X / \partial v_{DS}$ ,  $e_X^{(k)} = \partial f_X / \partial \Psi_S$ , all evaluated at  $\mathbf{x}^{(k)}$ , and  $r_X^{(k)} = f_X(v_{DS}^{(k)}, \Psi_S^{(k)}) - (c_X^{(k)} v_{DS}^{(k)} + e_X^{(k)} \Psi_S^{(k)}) - q_{X(n-1)}$ ,  $X = D$ , or  $S$ . Note that  $c_{\Psi}^{(k)} = e_D^{(k)} + e_S^{(k)}$  since  $f_{CH} = f_D + f_S$ .

## ACKNOWLEDGMENT

The author would like to thank N. Shanbhag for useful discussions.

## REFERENCES

- [1] D. O. Pederson, "A historical review of circuit simulation," *IEEE Trans. Circuits Syst.*, vol. 31, no. 1, pp. 103–111, Jan. 1984.
- [2] J. E. Meyer, "MOS models and circuit simulation," *RCA Rev.*, vol. 32, pp. 42–63, Mar. 1971.
- [3] D. E. Ward and R. W. Dutton, "A charge-oriented model for MOS transistor capacitances," *IEEE J. Solid-State Circuits*, vol. 13, no. 5, pp. 703–708, Oct. 1978.
- [4] S.-Y. Oh, D. E. Ward, and R. W. Dutton, "Transient analysis of MOS transistors," *IEEE J. Solid-State Circuits*, vol. 15, no. 4, pp. 636–643, Aug. 1980.
- [5] Y. Tsividis, *Operation and Modeling of the MOS Transistor*. 2nd ed. New York, NY, USA: Mc-Graw-Hill, 1999.
- [6] Y. Tsividis and C. McAndrew, *The MOS Transistor*. Oxford, U.K.: Oxford Univ. Press, 2012.
- [7] A. Raychowdhury, S. Mukhopadhyay, and K. Roy, "A circuit-compatible model of ballistic carbon nanotube field-effect transistors," *IEEE Trans. Comput.-Aided Design Integr. Circuits Syst.*, vol. 23, no. 10, pp. 1411–1420, Oct. 2004.
- [8] J. Deng and H.-S. P. Wong, "A compact SPICE model for carbon-nanotube field-effect transistors including nonidealities and its application—Part I: Model of the intrinsic channel region," *IEEE Trans. Electron Devices*, vol. 54, no. 12, pp. 3186–3194, Dec. 2007.
- [9] J. Deng and H.-S. P. Wong, "A compact SPICE model for carbon-nanotube field-effect transistors including nonidealities and its application—Part II: Full device model and circuit performance benchmarking," *IEEE Trans. Electron Devices*, vol. 54, no. 12, pp. 3195–3205, Dec. 2007.
- [10] Y.-Y. Chen, A. Sangai, M. Gholipour, and D. Chen, "Schottky-barrier-type graphene nano-ribbon field-effect transistors: A study on compact modeling, process variation, and circuit performance," in *Proc. IEEE/ACM Int. Symp. Nanoscale Arch. (NANOARCH)*, New York, NY, USA, pp. 82–88, Jul. 2013.
- [11] Y.-Y. Chen *et al.*, "A SPICE-compatible model of graphene nano-ribbon field-effect transistors enabling circuit-level delay and power analysis under process variation," in *Proc. Design Autom. Test Europe (DATE)*, Grenoble, France, Mar. 2013, pp. 1789–1794.
- [12] S. Frégonèse *et al.*, "Computationally efficient physics-based compact CNTFET model for circuit design," *IEEE Trans. Electron Devices*, vol. 55, no. 6, pp. 1317–1327, Jun. 2008.
- [13] M. Najari *et al.*, "Schottky-barrier carbon-nanotube transistor: Compact modeling, scaling study, and circuit design applications," *IEEE Trans. Electron Devices*, vol. 58, no. 1, pp. 195–205, Jan. 2011.
- [14] S. A. Thiele, J. A. Schaefer, and F. Schwierz, "Modeling of graphene metal-oxide-semiconductor field-effect transistors with gapless large-area graphene channels," *J. Appl. Phys.*, vol. 107, no. 9, May 2010, Art. ID 094505.
- [15] D. Jiménez and O. Moldovan, "Explicit drain-current model of graphene field-effect transistors targeting analog and radio-frequency applications," *IEEE Trans. Electron Devices*, vol. 58, no. 11, pp. 4150–4153, Nov. 2011.
- [16] D. Jiménez, "Explicit drain-current charge and capacitance model of graphene field-effect transistors," *IEEE Trans. Electron Devices*, vol. 58, no. 12, pp. 4377–4383, Dec. 2011.
- [17] I. N. Hajj, "Extended nodal analysis," *IEEE Trans. Comput.-Aided Design Integr. Circuits Syst.*, vol. 31, no. 1, pp. 89–100, Jan. 2012.
- [18] J. D. Lambert, *Numerical Methods for Ordinary Differential Equations: The Initial Value Problem*. Chichester, U.K.: Wiley, 1991.